Available online at www.sciencedirect.com

SciVerse ScienceDirect

Ceramics International 39 (2013) 2767–2774

CERAMICS INTERNATIONAL

www.elsevier.com/locate/ceramint

# Influence of crystallization inside glass frit on seal stress in ceramic metal halide lamps

Takuya Honma[a,*], Hiroshi Kamata[a], Junichi Tatami[b]

[a]Research and Development Center, Toshiba Lighting & Technology Corporation, 1-201-1 Yokosuka, Kanagawa 237-8510, Japan
[b]Graduate School of Environment and Information Sciences, Yokohama National University, 79-7 Yokohama, Kanagawa 240-8510, Japan

Received 13 June 2012; received in revised form 16 August 2012; accepted 12 September 2012
Available online 19 September 2012

**Abstract**

Ceramic metal halide lamps use polycrystalline aluminum oxide as an arc tube material; cracks inside the glass frit—used as the seal material—have been known to occur occasionally. This study measured the stress on the lamp seals caused by changes in the cooling rate during the sealing process by a 2D stress measurement method. Seal stress decreased with reducing cooling rate. Therefore, we discuss the influences of the glass frit's microstructure and the coefficients of thermal expansion (glass frit, capillary, and Nb wire) on the seal stress. The coefficient of thermal expansion of the annealed glass frit was essentially closer to those of the capillary and Nb wire, while that of the rapidly cooled glass frit differed greatly. Moreover, the glass frit of the rapidly cooled lamp seal contained only an amorphous phase (Dy, Si, Al, and O), while the glass frit of the annealed lamp seal contained both an amorphous phase (Dy, Si, Al, and O) and a crystalline one ($Dy_2SiO_5$ and $Al_2O_3$). Fracture toughness was found to be larger in the crystals than in the amorphous phase area. Moreover, it was larger in the area where crystalline $Dy_2SiO_5$ and $Al_2O_3$ were present compared to the area where only crystalline $Dy_2SiO_5$ was present.

Thus, the coefficient of thermal expansion of the glass frit containing the crystalline phase was found to influence the seal stress. Furthermore, the crystallization in the glass frit was found to influence crack propagation. Therefore, formation of cracks inside the glass frit can be prevented by optimizing these factors, which can be achieved by changing the cooling rate in the sealing process without changing the specifications of the glass frit (composition, composition ratio, etc.).


*Keywords:* Glass frit; Crack; Seal stress; Crystallization

## 1. Introduction

Glass frit is a material also referred to as sealing glass or solder glass. The material was originally derived from metallurgical techniques. The glass used to bind different glasses or to bind glass and metal is glass frit, and not a conventional optical material. Therefore, glass frit has been designed with the main focus being on the purpose of use [1]. In general, conventionally used glass frit is based on either a lead borate system or a lead borosilicate glass system. In particular, boro-aluminum-silicate glass, which is based on a borosilicate glass system, is used as an alternative material to those based on the lead glass system, owing to advancements in the lead-free movement in an effort by the entire industry with the aim of reducing the use of environmentally hazardous substances [1].

In terms of practical applications, glass frit has been used primarily for sealing metal. This sealing technology has gained importance because of its relevance to the development of light bulbs. Its importance has increased with the rapid development of the vacuum tube industry. In recent years, the microelectronics industry has witnessed some challenges with regard to the manufacture and design of packaging material. Therefore, the use of glass frit for sealing metal has attracted increasing interest in recent times; this has also garnered interest in other industries, such as those manufacturing solid fuel cells and biomedical products [2,3].

In particular, there has been a lot of interest in glass frit in the high intensity discharge (HID) lamp industry.

*Corresponding author. Tel.: +81 46 862 2154; fax: +81 46 860 1203.
*E-mail address:* takuya.honma@tlt.co.jp (T. Honma).

0272-8842/$ - see front matter © 2012 Elsevier Ltd and Techna Group S.r.l. All rights reserved.
http://dx.doi.org/10.1016/j.ceramint.2012.09.043

The reason is as follows: the recent increase in the operating temperature of these lamps for realizing higher luminance has led to an increase in the temperature of the arc tubes. The arc tubes of HID lamps were once made of silica glass, which has a glass transition point of 1150 °C. Therefore, the operating temperature of these lamps was restricted. In the early 1980s, polycrystalline aluminum oxide (PCA) began to be used for the arc tubes of metal halide lamps, which used metal halide materials for luminosity, as shown in Fig. 1a [4,5]. This alteration made it possible to achieve operating temperatures above 1150 °C, thus resulting in higher luminance. Owing to this improvement, the potential of glass frit for application to ceramic metal halide lamps was also studied. A high-pressure sodium (HPS) lamp, developed in the 1960s, was the first lamp to employ a ceramic arc tube. Around the same time, glass frit based on a $Re_2O_3$–$Al_2O_3$ system was also developed. Initially, ceramic metal halide lamps were developed using glass frit based on a $Dy_2O_3$–$Al_2O_3$ system. Although this lamp had acceptable performance, e.g., in terms of device lifetime, its manufacturing was difficult, in that its melting point was near or above 1800 °C. Several kinds of metal halides that have high vapor pressures and that are used as light-emitting materials are sealed inside ceramic metal halide lamps. Therefore, the sealing temperature for glass frit for this kind of lamp needs to be kept as low as possible to prevent the evaporation of metal halides. This problem led to the development of glass frit based on the $Dy_2O_3$–$Al_2O_3$–$SiO_2$ system, having a melting point near 1500 °C. Presently, this glass frit is widely used in ceramic metal halide lamps [6,7].

However, another problem occurs: cracks occasionally develop inside the glass frit (the material of the lamp seal), although the rate of their development is low. As shown in Fig. 1b, the crack progresses along the axial direction of the capillary. The crack, which poses a problem for the lamp, is developed from the glass frit end by the side of an arc tube to the glass frit end by the side of the Nb wire. Metal halide and fill gas inside an arc tube pass along this crack and are emitted outside. Consequently, lighting becomes impossible. A capillary, glass frit, and electrode constitute the seal of a ceramic metal halide lamp, as shown in Fig. 1a. The capillary—cylindrical in shape for ease of insertion in the electrode system—may be present at both ends of an arc tube. As mentioned above, the glass frit composition is based on the ternary system $Al_2O_3$–$Dy_2O_3$–$SiO_2$. The electrode system is composed of W, Mo, and Nb wires. The airtight seal used for the fill gas and metal halides is made of Nb wire with a small difference in the coefficients of thermal expansion (CTEs) of the glass frit and capillary. However, because different parts are sealed, the seal takes on different CTEs for three parts (glass frit, capillary, and Nb wire). Therefore, seal stress occurs easily under sealing and during operation, resulting in cracks. When the direction of progress of the crack is as shown in Fig. 1b, there is a high possibility of the seal stress being large in the axial direction of the capillary because of the large difference in the CTEs of the three parts in this axial direction.

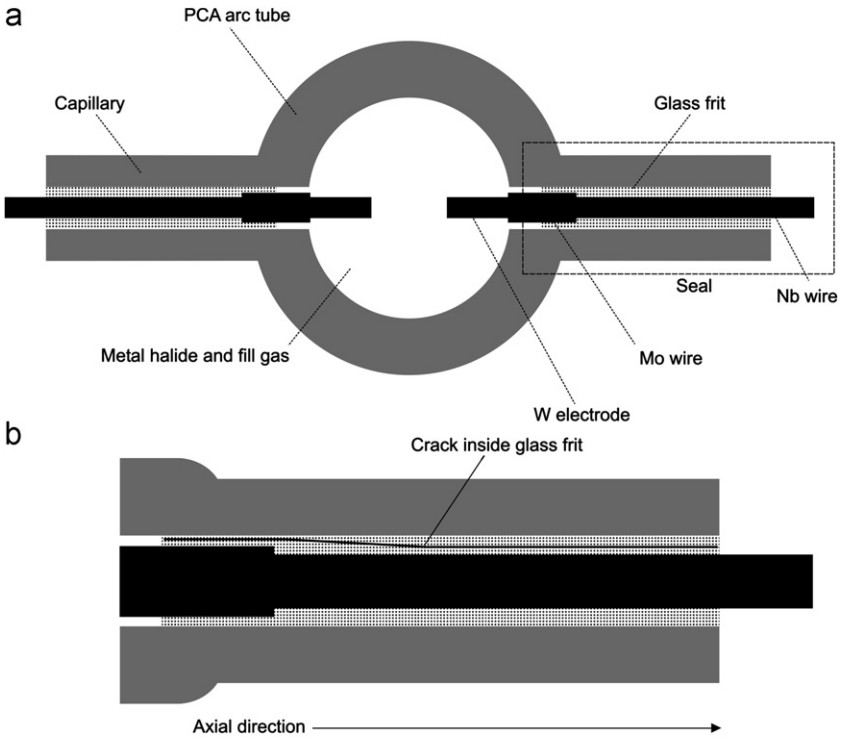


Fig. 1. Ceramic metal halide lamp. (a) Structure of ceramic metal halide lamp and (b) crack developed in axial direction inside the glass frit of seal.

The following are important requirements for glass frit: low viscosity, CTE matching that of the sample, high wettability, high chemical resistivity, high insulation, and high devitrification resistance. In particular, the requirement of CTE becomes important when the problem of crack generation explained above is focused on. Unlike those of metal, CTEs of glass frit yield a straight line at temperatures from room temperature up to the glass transition point ($T_g$); however, at temperatures above $T_g$, they do not yield a straight line. $T_g$ is the temperature at which glass frit changes from being in a rigid state to a viscoelastic state. Therefore, in the temperature region above $T_g$, glass frit is viscous, owing to which it is adaptable to the changes in the difference of shrinkage rate between the glass frit and the capillary, or the Nb wire, at the time of cooling. In contrast, at temperatures below $T_g$, when the difference in the shrinkage rate is large, cracks easily form in the glass frit. Ideally, there should be no difference in the CTEs between the glass frit and the capillary, or the Nb wire, at temperatures from the strain point to room temperature. However, this is not practically achievable [2].

Earlier studies have mainly investigated glass frit based on the $Al_2O_3$–$Dy_2O_3$–$SiO_2$ system in terms of its CTE, crystallization, and hardness [6–16]. For example, studies have been conducted on the influence of the composition ratio of glass frit on its CTE. As a result, it has been found that as the weight ratio of $SiO_2$ increases, the CTE decreases, and as the weight ratio of $Al_2O_3$ and $Dy_2O_3$ increases, the CTE increases. In particular, $Dy_2O_3$ is a dominant factor influencing the CTE [8]. In addition, heating of the glass frit results in the crystallization of the $Dy_2O_3$ and $Dy_2Si_2O_7$ contained in the glass frit. Further, relaxation of the residual stress inside the glass frit has also been studied, and it has been found that annealing for a fixed time results in relaxation of the internal residual stress of the glass frit at temperatures near $T_g$ [6,7].

However, seal stress has not yet been measured directly. Therefore, this study uses a 2D stress measurement method to measure the stress on lamp seals induced by changes in the cooling rate during the sealing process, and examines the factors influencing its value. It also assesses the effect of slower cooling rates and thereby discusses the influence of the microstructure inside the glass frit and of the CTE on seal stress. Moreover, through an investigation of fracture toughness, this study examines the relationship between crack progression and microstructure.

## 2. Material and methods

The lamp seal shown in Fig. 1a was used to investigate seal stress, the microstructure, and indentation-related fracture toughness. The average grain size of the PCA of the arc tube (G-40, NGK INSULATORS Ltd.) was 35 μm. The arc tube was of the spherical type, with an outside diameter of 8.00 mm and a thickness of 0.50 mm. Further, the capillary had an outer diameter of 1.80 mm, a thickness of 0.50 mm, and a length of 8.00 mm. Glass frit (G-66, NGK INSULATORS, Ltd.), which has a composition by weight of 16.8%% $Al_2O_3$, 61.4% $Dy_2O_3$, and 21.8% $SiO_2$, has a melting temperature of around 1390 °C. Nb wire with the additive of 1wt%-$ZrO_2$ (NbZr1%, W. C. Heraeus GmbH) was 0.70 mm in diameter and 10 mm in length. The seal of the glass frit was 9 mm in length.

In the sealing process, the samples were placed in the nitrogen-filled chamber and rapidly heated with a condensing infrared heater. Table 1 lists the conditions for the sealing process temperature profile, which includes the cooling and sealing steps. One sample was cooled rapidly (sample CR) and the other sample was annealed (sample A). The cooling rate ranged from 1600 °C to 1000 °C. The samples were cooled naturally below 1000 °C. After the sealing process, the cross section for the seal, shown in Fig. 2, was polished at its maximum diameter in the axial direction. The sample used for the investigation of CTE, which was fabricated using powder mixed in the same composition ratio as that in the glass frit and with the same temperature profile as that of the sealing conditions, is listed in Table 1. The fabricated bulk was processed into a $5 \times 5 \times 15\ mm^3$ size sample. In order to investigate the difference in the CTEs of the three parts (glass frit, capillary, and Nb wire) composing the seal, a capillary (8 mm in length) cut from the arc tube and the bulk of Nb (5 mm in outer diameter and 15 mm in length) were also prepared.

A μX-ray stress measurement method (D8 Discover with GADDS Bruker AXS Inc.) was used to investigate seal stress. In this measurement, we used a 2D stress measurement method that calculates stress from the distortion of the Debye–Scherrer ring image, as shown in Fig. 3 [17]. As shown in Fig. 1b, considering the direction of progress of the cracks, there is a high possibility of the difference in the CTEs between the three parts being larger in the axial direction of the capillary, which would result in

Table 1
Sealing process temperature profile of samples.

| Sample | Sealing step[a] | | Cooling step |
|---|---|---|---|
| | Sealing temperature (°C) | Sealing time (min) | Cooling rate (°C/min)[b] |
| Sample CR | 1600 | 1 | 600 |
| Sample A | 1600 | 1 | 75 |

[a]Samples were rapidly heated with a heater.
[b]Data are the values from 1600 °C to 1000 °C.

higher sealing stress. Therefore, when a sample was prepared for this measurement, its seal was cut and embedded in epoxy resin. Then, it was polished along the direction parallel to the axial direction of the capillary until it attained the maximum diameter of the cross section. The measurement points are shown in Fig. 2. This study intended to prioritize the measurement of stress in the axial direction of the capillary inside the sealing section because the crack progresses along the axial direction. Therefore, the stress measurement directions were the axial direction of the capillary and the radial direction perpendicular to it, as shown in Fig. 3, and the tangent stress in the circumference direction was not measured. The hatched region in Fig. 2 demonstrates the measurement area, which was $500 \times 500\ \mu m^2$, and the penetration depth of the X-ray, which was 400 nm. With regard to the measurement method, seal stress was measured by switching the values of $\chi$ and $\varphi$, as listed in Fig. 3 and Table 2, after measuring the Debye–Scherrer ring image at 136° of $Al_2O_3$ (146); $\chi$ is the rotation angle in the flapping direction of the sample, and $\varphi$ is the rotation angle in the horizontal direction of the sample. The stress was calculated by using an anisotropy coefficient of 1.0, a Young's modulus of 324 GPa, and a Poisson's ratio of 0.22. Moreover, the measured stress includes a seal stress generated by sealing, in addition to the residual stress present in the capillary before sealing. Therefore, the seal stress was calculated using the measured and residual stresses inside the capillary. Seal stress can be expressed as

$$S_S = M_S - R_S \quad (1)$$

where $S_S$ is seal stress (MPa), $M_S$ is measured stress (MPa), and $R_S$ is the residual stress inside the capillary(MPa). $R_S$ is the residual stress inside the capillary before sealing. The sample for $R_S$ measurement was fabricated and measured by the same method used for Sample CR and AN. The measured value was −18 MPa in the axial direction and −42 MPa in the radial direction. A positive value indicates a tensile stress, and a negative value indicates a compressive stress in the axial direction of the capillary.

The morphological observation and qualitative analysis are performed using an electron probe micro analyzer (EPMA) (SUPERPROBE, JEOL, Ltd.) in order to investigate the microstructure inside the glass frit. The microstructural analysis was also performed using a transmission electron microscope (TEM) (SIGMA, KEVEX Corp.). The solid region in Fig. 2 represents the measured area.

A micrometer method implemented with a laser length measuring machine (SL-2000M, SHINAGAWA REFRACTORIES Co., Ltd.) was used to investigate CTEs in the range of room temperature to 1000 °C.

A Vickers hardness tester (AVK-C2 Hardness Tester, AKASHI Corp.) and a scanning electron microscope

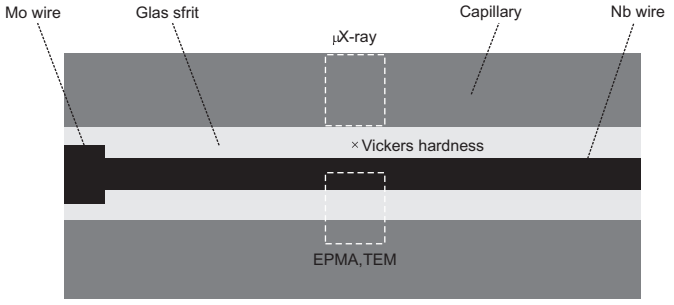


Fig. 2. Cross section of seal.

Table 2
Measurement condition in 2D method.

| $\chi$ (deg.) | $\varphi$ (deg.) |
|---|---|
| 0 | 0 |
| 45 | 0,45,90,135,180 |
| 60 | 0,45,90,135,180 |
| 75 | 0,45,90,135,180 |
| 90 | 0 |

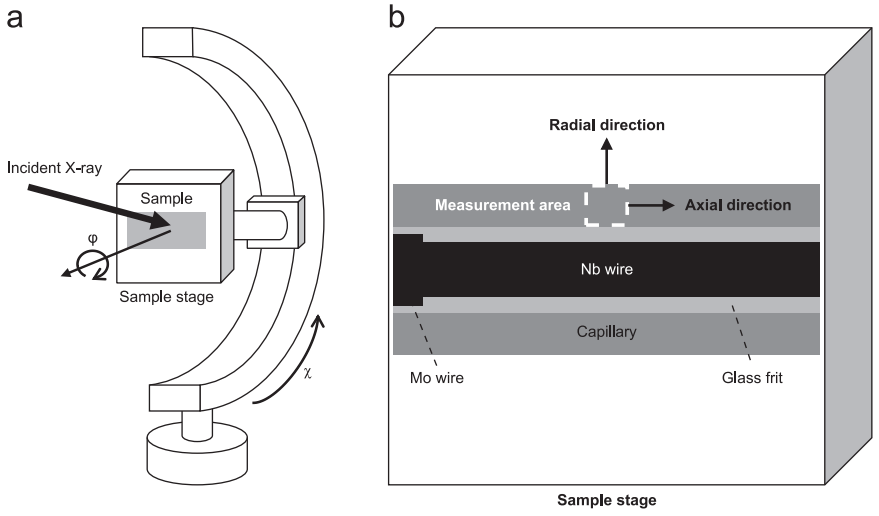


Fig. 3. μX-ray stress measurement using 2D stress measurement method. (a) Sample orientation in terms of $\chi$ and $\varphi$ angles and (b) measurement directions in stress.

(SEM) (SU-70, HITACHI, Ltd.) were employed to investigate fracture toughness inside the glass frit by the indentation fracture (IF) method. The cross region in Fig. 2 shows the measured area. Vickers hardness was measured using a load of 9.8 N. Moreover, the radius of the surface crack and the half-diagonal of the Vickers indent during the Vickers hardness test were measured using the SEM. The fracture toughness was calculated by using these measured values. It can be expressed [18] as

$$K_c = 0.203(a/c)^{3/2} H_v\, a^{1/2} \quad (2)$$

where $K_c$ is the fracture toughness (Pa $m^{1/2}$), $c$ is the radius of the surface crack ($m$), $a$ is the half-diagonal of the Vickers indent ($m$), and $H_v$ is the Vickers hardness (Pa). In this investigation as well as that of seal stress, $c$ and $a$ in the axial direction of the capillary were measured.

## 3. Results and discussion

The measured results of seal stress are presented in Table 3. To determine the measurement errors according to the measurement method, 2 samples were measured 3 times, using the same portions for each sample. The average of the measured values and standard deviations ($3\sigma$) are shown. These results indicate that tensile stress was produced inside the capillary in the axial direction after the sealing process, regardless of the cooling rate, although seal stress did not occur in the radial direction. The CTEs of the glass frit, capillary, and Nb wire were found to influence this outcome. Further, the generation of stress began in the cooling step during the sealing process, in the temperature range where the glass frit changed from being in the viscoelastic state to being in the rigid state, i.e., when it went below $T_g$ [2]. Fig. 4 shows the measurement results of the CTE, which indicate that $T_g$ of the glass frit was in the vicinity of 800 °C. Furthermore, the lamps were designed such that when they were operated, the operating temperature of the seal was also maintained below $T_g$. Therefore, the relationship between the CTEs of the Nb wire, the capillary, and glass frit at temperatures below 800 °C was discussed. The capillary and glass frit were used as examples to explain the effects of the CTE on the seal stress. The measurement results indicate that the CTE of the capillary was larger than that of the glass frit. The seal stress was produced by the difference in CTEs between the capillary and the glass frit. The two shrunk in the cooling step performed after the sealing step. However, the shrinkage rate of the capillary is larger than that of the glass frit. Therefore, although the capillary would have shrunk more than the glass frit, the glass frit prevented the capillary from actually shrinking. Consequently, the tensile stress inside the capillary and the compressive stress inside the glass frit counteracted each other. Therefore, the seal stress is produced between the capillary and the glass frit. The higher the difference in the CTEs of these parts in the cooling step, the higher this counteraction. In connection with this mechanism, the seal stress also increases. Moreover, in the case of taking into consideration the difference in CTEs between the capillary and the glass frit, there is a high possibility of a similar phenomenon occurring between the Nb wire and the glass frit.

Table 3
Seal stress measured by μX-ray stress measurement.

| Sample | $S_S$ (MPa)[a] | |
|---|---|---|
| | Axial direction | Radial direction |
| CR | $45 \pm 7$ | $0 \pm 6$ |
| A | $30 \pm 7$ | $-1 \pm 6$ |

[a]Values are average of measured values and standard deviation ($3\sigma$).

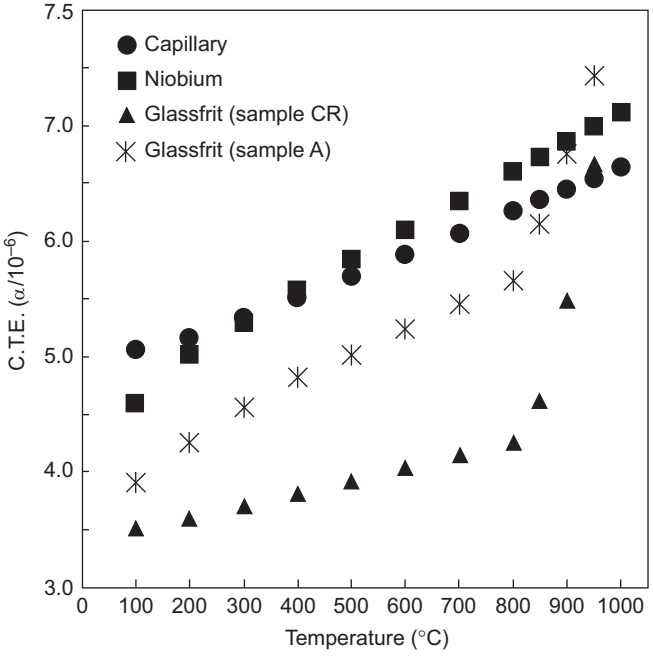


Fig. 4. Coefficient of thermal expansion versus temperature.

Moreover, the seal stress in the axial direction of sample A decreased by 33% relative to that of sample CR. The standard error for sample CR was 7 MPa and that for sample A was 5 MPa in the axial direction. Based on the $3\sigma$ and standard errors, it was determined that the samples were not very different with regard to seal stress in the axial direction. Therefore, $t$-test was performed to statistically analyze the difference. Since $t$-boundary value at both sides (2.7764) had exceeded $t$-absolute value (1.6821), it was judged that difference between sample CR and A in the axial direction existed.

As stated above, it appears that the difference in the CTE between the glass frit of the two samples in the cooling step has an influence on seal stress in the axial direction. Fig. 4 shows that the CTE of the glass frit of sample A was essentially close to those of the capillary and Nb wire; however, the CTE of the glass frit of sample CR differed

greatly. The difference in the CTE of the glass frit of samples CR and A was influenced by the microstructure.

Fig. 5 shows SEM images of the microstructure inside the glass frit of the lamp seals. The crystal was not detected by the morphological observation of sample CR. The elements Dy, Si, Al, and O of the glass frit were identified by qualitative analysis. The black and white crystals in the matrix (Dy, Si, Al, and O) of sample CR were detected by the morphological observation of sample A. The crystal constituted about 70% of the glass frit. The Al and O contents of the black crystal and the Dy, Si, and O contents of the white crystal were detected by qualitative analysis. Furthermore, the crystal structure was investigated by electron diffraction in the TEM. It can be expressed as

$$Rd = L\lambda \tag{3}$$

where $R$ is the distance from a standard point (000) of a diffraction spot (cm), $d$ is a lattice plane space corresponding to the diffraction spot (Å), $L$ is the distance between the camera of the TEM and a sample (160 cm), and $\lambda$ is the electron beam wavelength (0.0251 Å). The crystal structure was determined by measuring the lattice plane space and the angle between the diffraction spots, and also on the basis of the result of the qualitative analysis. Only sample A was used in this investigation. Although this sample equaled that inspected by the EPMA, it was in another area. The TEM image is shown in Fig. 6a. Electron diffraction was used to investigate the portion in A where the crystal was not

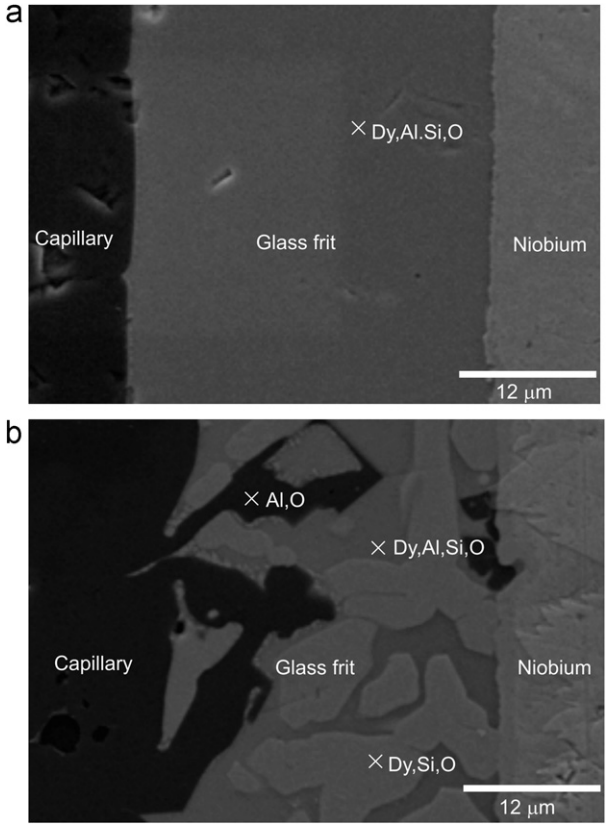


Fig. 5. Scanning electron microscope image of seal. (a) Sample CR and (b) sample A.

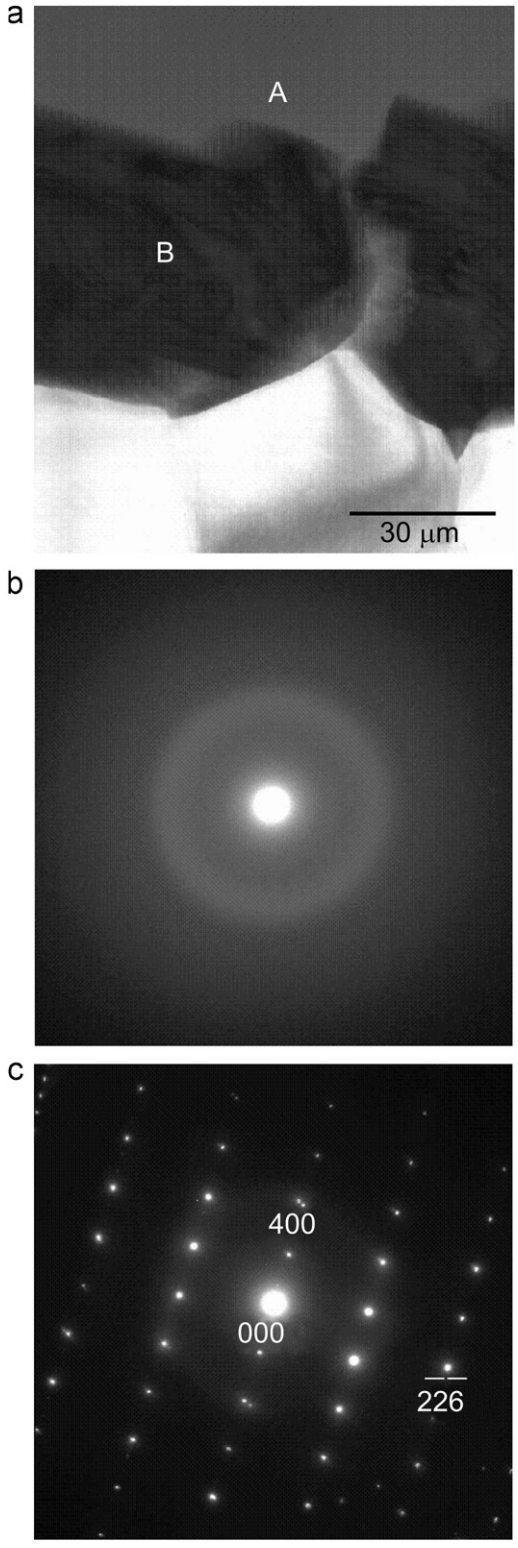


Fig. 6. Electron diffraction in transmission electron microscope (sample A). (a) TEM image, (b) measurement portion in A and (c) measurement portion in B.

detected and the portion in B with the white crystal. The black crystal had a high possibility of possessing crystalline $Al_2O_3$. The result revealed that the portion in A was of an amorphous phase with a hollow pattern, as shown in Fig. 6b.

The portion in B showed an electron diffraction pattern (see Fig. 6c) that originated in the crystal and was identified as crystalline $Dy_2SiO_5$. Therefore, since the CTE of the glass frit of sample A, on which the crystals ($Dy_2SiO_5$ and $Al_2O_3$) were present, was larger than that of sample CR, which did not crystallize, the former CTE approached those of the capillary and Nb wire. As a result, the seal stress of sample A decreased by 33% relative to that of sample CR. Moreover, as shown in Fig. 5b, the crystalline $Al_2O_3$ detected in sample A grew radially and anisotropically from the capillary. This growth possibly occurred because the crystal of $Al_2O_3$ composing the glass frit grew from the surface of the capillary as crystalline nuclei in the cooling step during the sealing process. As shown in Fig. 1b, the crack progresses along the axial direction of the capillary. Therefore, the progress of the crack of the axial direction can be prevented by the crystal of $Al_2O_3$ grew from the surface of the capillary. Moreover, it is highly possible that these alumina crystals play a role in gradient function, which relaxed the difference in seal stress between the capillary and glass frit [16].

The SEM images of the indentation and the crack at the corner produced by the Vickers hardness are shown in Fig. 7, and the measured result of $K_c$ is presented in Table 4. The amorphous phase was investigated by using sample CR, and the crystal was investigated by using sample A. Two areas containing the amorphous phase in sample A were studied: one where crystalline $Dy_2SiO_5$ was present and the other where crystalline $Dy_2SiO_5$ and $Al_2O_3$ were present. Although these two areas are part of the same sample, their cooling rates are different owing to the differences in thermal conduction in these areas in the cooling step. Therefore, despite being on the same sample, these two areas have different crystallization states. However, in order to investigate the influence of IF on crystalline $Al_2O_3$, it was necessary to investigate the areas in which the crystalline state differs. As a result, $K_c$ of the area in which crystals were present was found to be larger than that in which only the amorphous phase was present. Moreover, $K_c$ of the area in which crystalline $Dy_2SiO_5$ and $Al_2O_3$ were present was larger than that of the area in which only crystalline $Dy_2SiO_5$ was present. The crack crossed both the amorphous and crystal phases and had been formed not at the interface between the two phases but in the crystal grains. The direction of crack progression in the crystals tended to change, and this tendency was especially remarkable in the area containing crystalline $Al_2O_3$. $H_v$ has an influence on this phenomenon. The $H_v$ value of the area in which crystalline $Dy_2SiO_5$ and $Al_2O_3$ existed was higher than those of the amorphous phase and the area in which crystalline $Dy_2SiO_5$ existed. As a result, $H_v$ of crystalline $Al_2O_3$ appears to be higher than those of the amorphous phase and crystalline $Dy_2SiO_5$. Therefore, the crystal of $Al_2O_3$ seems to have suppressed crack progression, which in turn influenced fracture toughness. Moreover, the $Al_2O_3$ crystals grew radially and anisotropically from the capillary. The crack inside the glass frit progressed in the axial direction of the capillary. In the case of this crystallization pattern, there is a strong possibility that the crack was suppressed, which also affected fracture toughness.

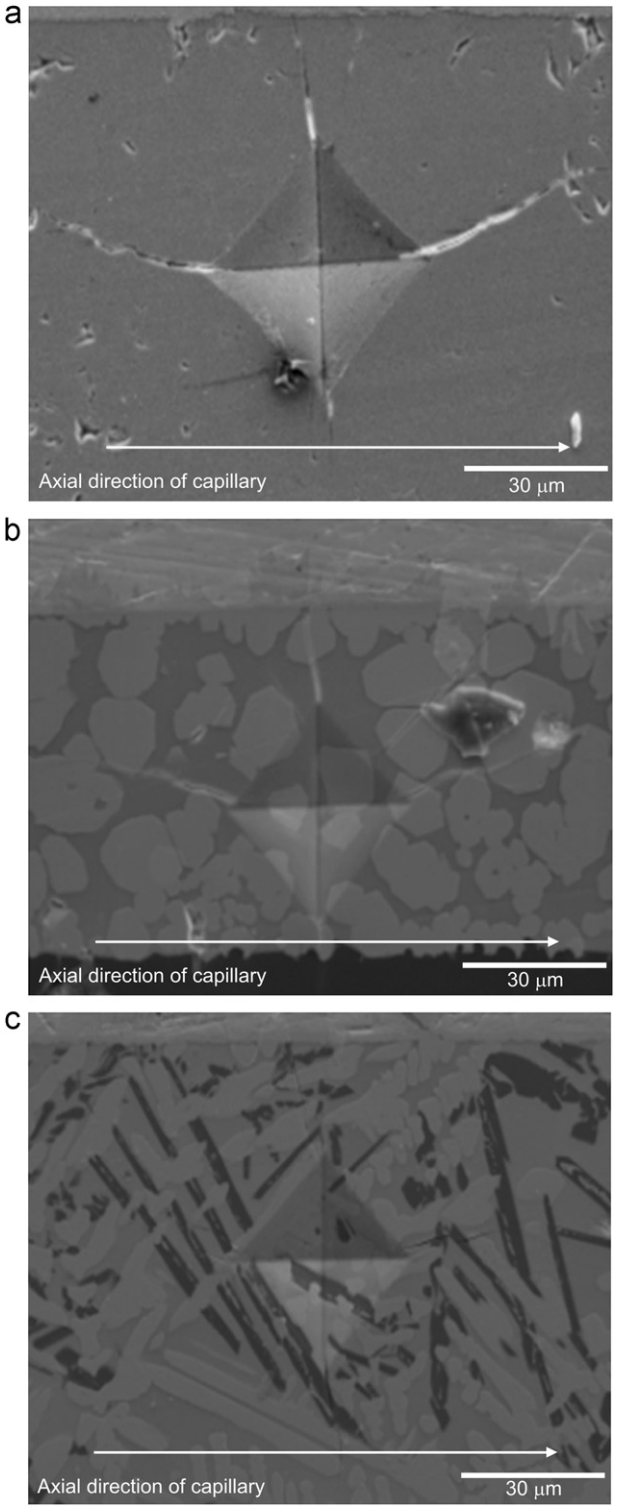


Fig. 7. Scanning electron microscope image of the indentation and the crack produced by Vickers hardness on the corner. (a) Only amorphous phase (Sample CR), (b) Area where $Dy_2SiO_2$, is present (sample A) and (c) Area where $Dy_2SiO_2$, is present (sample A).

Table 4
Fracture toughness by the indentation fracture method.

| Measurement area | $H_v$ (GPa) | $a$ (μm) | $c$ (μm) | $K_c$ (MPa $m^{1/2}$) |
|---|---|---|---|---|
| Amorphous | 8.3 | 25 | 61 | 2.2 |
| $Dy_2SiO_5$ | 13.6 | 19 | 55 | 2.5 |
| $Dy_2SiO_5$, $Al_2O_3$ | 14.7 | 18 | 31 | 5.7 |

## 4. Conclusions

In this study, we measured the dependence of lamp seal stress on changes in the cooling rate during the sealing process by a 2D stress measurement method. Seal stress was found to decrease with reducing cooling rate. We also discussed the influence of the microstructure inside the glass frit and the coefficients of thermal expansion (glass frit, capillary, and Nb wire) on seal stress. Moreover, we revealed the relation between crack progression and the microstructure through an investigation of fracture toughness. Through this research, we arrived at the following conclusions:

(1) The coefficient of thermal expansion of the annealed glass frit was relatively close to those of the capillary and Nb wire, while that of the rapidly cooled glass frit differed greatly.
(2) The glass frit of the rapidly cooled lamp seal was found to contain only the amorphous phase (Dy, Si, Al, and O), and that of the annealed lamp seal was observed to contain crystalline $Dy_2SiO_5$ and $Al_2O_3$ within the amorphous phase.
(3) The fracture toughness of the area in which crystals were present was larger than that of the area in which only the amorphous phase was present. Moreover, the fracture toughness of the area in which crystalline $Dy_2SiO_5$ and $Al_2O_3$ were present was larger than that of the area where only crystalline $Dy_2SiO_5$ was present.

Thus, the CTE of the glass frit containing the crystalline phase was found to influence the seal stress. Furthermore, the crystallization in the glass frit was found to influence crack propagation. Therefore, the formation of cracks inside the glass frit can be prevented by optimizing these factors, which can be achieved by changing the cooling rate in the sealing process without changing the specifications of the glass frit (composition, composition ratio, etc.).

## References

[1] V.K. Shrikhande, Preparation and characterization of special glasses for sealing and other applications, IOP Conference Series: Materials Science and Engineering 2 (2009) 012016.
[2] R.G. Frieser, A review of solder glasses, Electrocomponent Science Technology 2 (1975) 163–199.
[3] I.W. Donald, P.M. Mallinson, B.L. Metcalfe, L.A. Gerrard, J.A. Fernie, Recent developments in the preparation, characterization and applications of glass- and glass-ceramic-to-metal seals and coatings, Journal of Materials Science 46 (2011) 1975–2000.
[4] S. Jungst, D. Lang, and M. Galvez, Improved arc tubes for ceramic metal halide lamps, Proceedings of the 10th International Symposium on the Science and Technology of Light Sources, Toulouse, France, July 18–22, 2004.
[5] T.G.M.M. Kappen, Ceramic metal halide lamps: a world of lighting, Proceedings of the 10th International Symposium on the Science and Technology of Light sources, Toulouse, France, July 18–22, 2004.
[6] Y. Liu, Z. Geng, W. Zhuang, H. He, Study on thermal expansion behavior of $Dy_2O_3$–$Al_2O3$–$SiO_2$ glass, Journal of Rare Earth 26 (2008) 85–88.
[7] Z. Geng, Y. Liu, X. Liu, Expansion coefficient of sealing material for ceramic metal halide lamps, Key Engineering Materials 368–372 (2008) 1603–1605.
[8] Y. Liu, Z. Geng, W. Zhuang, H. He, Study on thermal expansion coefficient of sealing materials for ceramic metal halide lamps, Journal of Rare Earth 25 (2007) 249–252.
[9] G. Dobos, K.V. Josepovits, Z. Tóth, I. Csányi, L. Kocsányi, Surface analytical study of the ceramic-metal bond in the electrical feed-through of high pressure sodium lamps, Proceedings of the 11th International Symposium on the Science and Technology of Light Sources, Shanghai, China, May 20–24, 2007.
[10] H. Takashio, Translucent aluminum oxide-to-niobium metal seals by solder glass in the system CaO–$Al_2O_3$–$SiO_2$–MgO, Yogyo Kyokai Shi 80 (1972) 163–172.
[11] H. Takashio, Translucent aluminum oxide-to-niobium metal seals using a crystalline solder in the system CaO–$Al_2O_3$–MgO–$B_2O_3$, Yogyo Kyokai Shi 84 (1976) 420–425.
[12] H. Takashio, Translucent aluminum oxide-to-niobium metal seals by a modified solder glass technique using an adhesive in the system CaO–$Al_2O_3$–$SiO_2$–MgO, Yogyo Kyokai Shi 82 (1974) 248–256.
[13] S.M. DeCarr, J.C. Grande, M. Gyor, I. Laher, D.J. Lovett, J. Meszaros, Characterizing metal-to-ceramic seals for high intensity discharge lamps, Proceedings of the 9th International Symposium on the Science and Technology of Light Sources, New York, USA, August 12–16, 2001.
[14] N. Brates, D. Goodman, J. Maya, Y. Nishimura, N. Takeuchi, Salt-frit reactions in ceramic metal halide lamps, in: Proceedings of the 10th International Symposium on the Science and Technology of Light Sources, Toulouse, France, July 18–22, 2004.
[15] Z. Tóth, A. Juhász, B. Nyiri, Evaluation of the mechanical properties of HID sealing during ageing, in: Proceedings of the 9th International Symposium on the Science and Technology of Light Sources, New York, USA, August 12–16, 2001.
[16] Z. Tóth, Z. Koltani, G. Steinbach, A. Juhász, K. Váradi, Residual stress anisotropy in high pressure sodium lamp seals, Journal of Physics D: Applied Physics 38 (2005) 3047–3056.
[17] Y. Sakaida, Study on minimum irradiation area and microstructure in micro X-ray stress measurement, Journal of the Society of Materials Science 53 (2004) 758–764.
[18] B.R. Lawn, E.R. Fuller, Equilibrium penny-like cracks in indentation fracture, Journal of Materials Science 10 (1975) 2016–2024.